Journal of Cleaner Production 269 (2020) 122157

Contents lists available at ScienceDirect

Journal of Cleaner Production

journal homepage: www.elsevier.com/locate/jclepro

Recycling of polymer laminated aluminum packaging (PLAP) materials into carbonaceous metallic microparticles

Abdullah Al Mahmood [a], Rumana Hossain [a, *], Saroj Bhattacharyya [b], Veena Sahajwalla [a]

[a] Centre for Sustainable Materials Research and Technology, SMaRT@UNSW, School of Materials Science and Engineering, UNSW Sydney, Australia
[b] Mark Wainwright Analytical Center, UNSW, Sydney, NSW, 2052, Australia

ARTICLE INFO

Article history:
Received 29 January 2020
Received in revised form
7 May 2020
Accepted 9 May 2020
Available online 22 May 2020

Handling Editor. Meisam Tabatabaei

Keywords:
Aluminum recycling
Packaging waste
Polymer degradation
Cryo-milling
Aluminum microparticles

ABSTRACT

This research describes the recycling of laminated metal packaging into multiple products by utilizing three different techniques. PLAP materials have been thermally disengaged at 550 °C for 20 min in an argon gas created inert atmosphere to recycle into solid Al and graphitic carbon. In a different route, in the presence of gaseous N_2 at 600 °C for 1h, the PLAP materials are degraded into bio-oil. A new technique to produce powdered materials from the ductile metal (Al) has been introduced in this study. In this technique, recycled Al and C from the first route at 550 °C, undergoes mechanical milling at cryogenic temperature (−196 °C) created by liquid N_2. The translatory high energy ball milling process varied for 2, 4, 6, and 8 cycles (time: 17, 29, 41, and 53 min respectively). As the milling process is extensively high impact loaded at a very low temperature, the foil-like Al recycled from the packaging waste transforms into smaller particles within a very short time (20 min). Upon further milling (41 min), the microparticles (particle size below 100 μm) of Al can be observed. The microparticles received from the cryo-mill are characterized to investigate the particle size, morphology, crystallographic structure, thermal behavior, chemical state, and dispersibility in different liquid media. Flake shaped, and micro-sized carbonaceous Al microparticles are contamination-free and thermally stable and can be useful in the fields of additive manufacturing.

1. Introduction

The wide range of applications of aluminum powder upsurge the interest of fabrication of this essential metal into powder form by several conventional and unconventional powder fabrication techniques. There is a growing market for aluminum powder in the field of applications in paint, slurry, explosives, protective coatings, pigments, rocket fuel, printing inks, abrasives, and ceramics, etc. (Primary Information Services, 2018). The market of aluminum powder in 2017 was valued at 3 billion USD and it is expected to reach 3.92 billion USD by 2025 (P.M. Research, 2018).

The conventional way of producing aluminum powder is molten metal atomization (Williams, 1984; Cox et al., 1978). In addition, there are some other techniques of metal powder production like chemical synthesis (Haber and Buhro, 1998), wire explosion by electricity (Tepper, 2000; Kwon et al., 2001; Sarathi et al., 2007), condensation of gas (Gutmanas et al., 1994; Sánchez-López et al., 1998; Groza, 1999), hydrogen plasma evaporation (Sun et al., 1999), DC plasma arc (Hull, 2002), laser induction complex heating (Guo et al., 2008), arc plasma spraying (Mandilas et al., 2013), transferred arc thermal plasma reactor (Pant et al., 2016), and radiofrequency induction plasma (Karthik et al., 2018). To produce fine grade (5–100 μm) aluminum powder mechanical milling is a more realistic method. By this method, micron size powder can be produced quickly though it is possible to produce nano-size metal powder by ball-milling for a long time in an inert atmosphere (Khan et al., 2008). In mechanical ball-milling particles are subjected to the impact loading causes fracture to the particles. Upon further milling, the particles are cold-welded together and again flattened and fractured to the smaller particle size (Suryanarayana, 2001). Even though the mechanical ball milling can produce fine metallic powders, He et al. suggested that the mechanical ball milling can change the deformation mechanism for the FCC materials (e.g. aluminum) by induced deformation twinning (He et al., 2003).

Cryo-milling is the technique to produce a large quantity of

* Corresponding author.
E-mail addresses: m.almahmood@unsw.edu.au (A. Al Mahmood), r.hossain@unsw.edu.au (R. Hossain), veena@unsw.edu.au (V. Sahajwalla).

https://doi.org/10.1016/j.jclepro.2020.122157
0959-6526/

Nomenclature

Al_2O_3	Aluminum oxide
A$	Australian dollar
DBT	Ductile to brittle transformation
DTG	Derivative of thermogravimetry
FCC	Face centered cubic
FE-SEM	Field emission electron microscopy
FTIR	Fourier transform infrared spectroscopy
GC-MS	Gas chromatograph-mass spectrometer
ICP	Inductively coupled plasma
MSW	Municipal solid waste
PET	Polyethylene terephthalate
PP	Polypropylene
PLAP	Polymer laminated aluminum packaging
SAED	Selected area electron diffraction
TDT	Thermal disengagement technology
TEM	Transmission electron microscopy
TGA	Thermogravimetric analysis
XPS	X-ray photoelectron spectroscopy
XRD	X-ray diffractometry

metal powder in the relatively shortest period of time, where mechanical milling is carried out at extremely low temperatures (−196 °C) created by liquid nitrogen (Kumar and Biswas, 2017). Koch C.C shows that by reducing the milling temperature the grain size of the metal powder can be reduced remarkably (Koch, 1989). Along with the temperature, there is a huge effect of milling time on the size of the fabricated particles. From the research of Nirmal K et al. it can be observed that at the cryogenic temperature, the increase of milling time leads the particles to finer grain size (Kumar and Biswas, 2017). Moreover, the type of the balls, the diameter of the balls, balls to powder weight ratio, and speed of rotation/vibration have a significant effect on the type and characteristics of the metal powders. Cryo-milling leaves no hazardous residues and by-products so it can be called a clean fabrication technique. It has less contamination from the milling media compared to the traditional room temperature ball milling due to the quick milling time. At low-temperature milling, there is a minimum chance to get oxidation and it can be further minimized by using inert gas and the possibility of cold welding by adhesion of the fine particles can be minimized by using some surfactants (Enayati, 2017).

From the life cycle assessment of Al-Polymer packaging materials done by Xie et al., it is clearly found that the metalized packaging materials are mostly ended with landfilling, followed by the incineration with other municipal solid waste (MSW), and the rate of recycling is almost negligible (Xie et al., 2016). Thin PLAP waste materials recycling is always a difficult task as the surface area of the thinner materials is higher in comparison to the bulk material and it exposes more to the atmospheric oxygen. Aluminum is very sensitive to oxygen and it can react with atmospheric oxygen to form a thin oxide layer and the rate of oxidation at elevated temperature is higher than that of room temperature oxidation (Rai et al., 2006; Blackburn and Gulbransen, 1960). Thus, the recycling of thinner aluminum waste packaging is difficult in traditional smelting methods. Yin et al. proposed a thermal route of recycling packaging waste materials containing several polymers and aluminum, with the yield of the metallic aluminum was 30% with ~95% purity (Yin et al., 2019a). On a different platform, Siddiqi et al. utilized thin metalized packaging materials to produce good quality oil by pyrolysis (Siddiqui et al., 2019). Our previous work describes the thermal transformation of the polymer-metal packaging materials into considerably pure metal and graphitic carbon particles by thermal disengagement technology (TDT) (Al Mahmood et al., 2019). Thermal disengagement technology utilizes the optimum conditions to transfer the waste materials into its original or any other beneficial forms suitable for further applications. The synthesis of aluminum microparticles from the recycled scrap packaging materials is still a challenge for the researchers.

In this research, two different routes for the thermal disengagement of the PLAP materials are investigated. (1) Thermal degradation of the PLAP materials at 550 °C in an argon gas created inert atmosphere to recycle the materials into Al and C, and (2) Pyrolytic degradation of the polymer laminates with the PLAP materials at 600 °C in gaseous N_2 atmosphere to synthesis polymer degraded oil. Recycled aluminum from route 1 with the graphitic carbonaceous materials from the waste PLAP materials is cryo-milled at the different conditions to optimize the process parameters. But, the main significance of this analysis is to find out a non-traditional way of powder production of the FCC material (Al), which is not in practice to date as this type of materials does not undergo any ductile to brittle transformation (DBT) at a lower temperature, when Al is in bulk condition. Our study material has a very thin cross-section and behaves like Al foil. When it is mechanically milled at the ultimate low temperature created by liquid N_2, ductile Al becomes finer flake shaped particles like any other brittle materials. Even though this cryo-milling process is not suitable for bulk Al, it can be potentially utilized for thin foil Al to produce microparticles even nanoparticles at a longer milling time. Ultimately, the process ended up with the conclusion of a clean recycling process of the laminated metal (Al) packaging into powdered metal, as no additive materials are used and no hazardous residue leaves from this processing technique.

2. Materials and methods

2.1. Thermal processing and oil synthesis

The raw material for this research is post-consumer coffee pods, collected from the community coffee shops. They were shredded into smaller pieces and thereby the coffee grounds, some external materials, and the metallic parts were separated. The laminated metallic part was thermo-disengaged at 550 °C for 20 min in a horizontal tube furnace (Radatherm, HTF 7060) in an inert atmosphere created by argon purge (1 L/min). Laminated polymers were degraded into carbonaceous materials by the degradation and volatilization of the moistures and other gaseous molecules from the polymers. Moreover, the polymer-metal packaging material was pyrolyzed in a furnace at 600 °C for 1h in nitrogen (N_2) atmosphere, and a brown oil was collected in the condenser of the pyrolysis setup (represented in Fig. 1). Collected oil was diluted in acetone for qualitative analysis in a gas chromatograph-mass spectrometer (GC-MS, 1200L Single Quad, Varian Inc.).

2.2. Aluminum microparticles synthesis

Thermo-disengaged (in argon media) PLAP materials were cryo-milled (Retsch cryomill, Germany) in a cryogenic temperature (−196 °C) created by the continuous supply of liquid nitrogen. The function of a cryo-mill is to grind feed materials in a cryogenic condition created by liquid nitrogen from an integrated cooling system before and during the grinding process. The sample embrittlement happens through the continuous flow of liquid nitrogen from an automated filling system (RetschCryoMill, 2018). Fig. 2 shows the schematic representation of a cryo-mill used for the experiment and the detail parameters of the cryo-milling are summarized in Table 1.

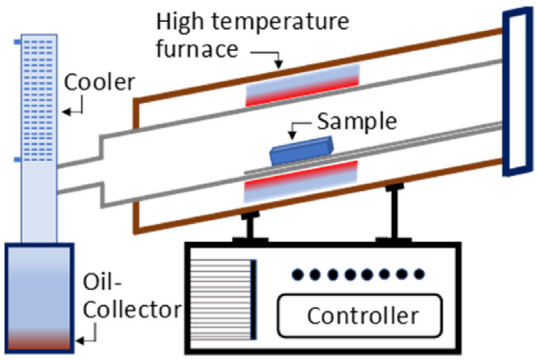

Fig. 1. Schematic of the pyrolysis setup.

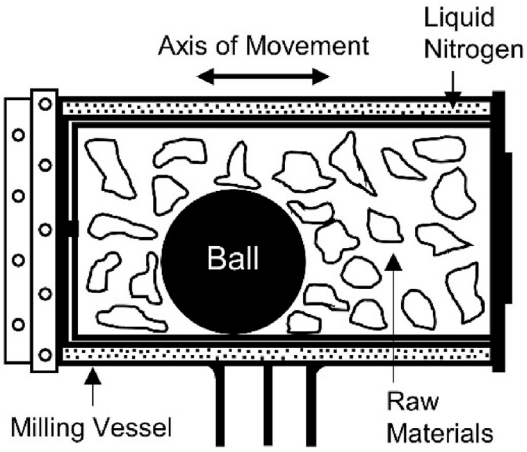

Fig. 2. Schematic of the cryo-mill.

2.3. Characterizations

The degradation characteristics of the PLAP materials under the influence of heating in an inert atmosphere was characterized by the thermogravimetric analyzer (TGA, STA-8000, PerkinElmer). The sample was heated from 30 °C to 900 °C at a heating rate of 20 °C/min in a closed chamber in a controlled environment with the continuous flow of gaseous nitrogen (flow rate: 20 ml/min) and cooled down to the atmospheric temperature with the same rate and conditions. The ICP-MS technique was used to estimate the composition of the metal (Al) after the thermal disengaged.

Two scanning electron microscopes were used to investigate the morphology and microstructures of the fabricated aluminum powders. For low magnification imaging Hitachi S3400 and for high magnification imaging field emission electron microscope Nova Nano SEM-450 were used. The nano FE-SEM 450 allows achieving high imaging resolution at both fields free and immersion mode of imaging for compressive low to high resolution. The powders were initially coated with platinum by LEICA EM ACE-600 sputter coater for better resolution.

Table 1
Parameters for cryo-milling.

Parameters	Specific details
Milling ball	Diameter: 25 mm Material: Stainless steel
Milling jar	Capacity: 50 ml Material: Stainless steel
Principle	Impact, friction
Ball to feed materials ratio	35:1
Vibrational frequency	5 per second
Milling cycles	2, 4, 6, and 8
Milling time	17, 29, 41, and 53 min

The particle size distributions of the synthesized powders were characterized by a laser diffraction particle size analyzer (Malvern Panalytical, Mastersizer-3000). The size distribution of the powder samples was measured using a wet dispersion technique. The medium of dispersion for the powder sample for mastersizer-3000 can be water or ethanol. Aluminum powder dispersion in ethanol found better compared to the dispersion in water. So, ethanol was used as a dispersion media to analyze the particle size distribution of the fabricated aluminum powders.

Structural analysis and the phase relationship of the fabricated powders were characterized by X-ray diffractometer (MPD, Panalytical, Xpert Multipurpose X-Ray Diffraction system) using CuK_{α} radiation ($\lambda = 1.541874$ Å, 45 kV, 40 mA) with scan range 5–140°, step size 0.0130 and scan time per step 233 s. Apart from the phase fractions, the quantitative analysis including crystallite size and micro-strain analysis of the powder samples were estimated by X'pert high Score Plus (Panalytical) software.

The chemical state of the surface of the fabricated aluminum powders was characterized by using Thermo ESCALAB250Xi X-ray photoelectron spectrometer (XPS) with the depth profile and elemental imaging. The source of the x-ray was mono-chromated aluminum Kα. The photoelectron signals from the surface of the samples were detected at a 90° angle to enhance the detection sensitivity in a high vacuum chamber.

Thermogravimetric analysis of the fabricated powder samples was carried out with the same instrument mentioned earlier (PerkinElmer Simultaneous Thermal Analyzer (STA-8000)) in an atmosphere with a continuous flow of nitrogen at 20 ml/min. The material was heated from 30 °C to 700 °C in an alumina crucible at 20 °C/min and then it was cooled down to the initial temperature at a cooling rate 20 °C/min.

To analyze the microstructure and the crystallinity of the fabricated powders Tecnai-G220 and the Philips CM-200 field emission transmission electron microscopes (TEM) were used. Samples were sonicated in methanol media for 2 min and then one drop of the mixture was added directly on the copper grid. The grid with the powder droplets was kept overnight in a desiccator to avoid oxidation and to remove the methanol from the grid. Copper grids were loaded into the transmission electron microscopes by a single tilt holder for the analysis.

3. Results and discussion

3.1. Characterization of raw and thermo-disengaged PLAP materials

The degradation characteristics of the PLAP materials at elevated temperatures were analyzed by TGA in a nitrogen atmosphere (20 ml/min) with a heating rate of 20 °C/min. Fig. 3 represents the thermal degradation characteristics of the PLAP materials in the temperature ranges 30°C–900 °C, where the curve denoted by 'TGA' (thermogravimetric analysis) represents the percentage of weight reduction upon the temperature increases, 'DTG' identifies the points where the mass degradation occurs significantly, and the curve represented by the 'heat flow' shows the endothermic/exothermic heat flow characteristics of the PLAP materials at different temperatures. Polymeric decomposition can be observed in two distinguished regions clear evidence from the 'DTG' curve with two peaks at 325 °C (slope: $-2.62e^{-4}\pm1.23e^{-6}$, intercept: $0.06\pm3.7e^{-4}$) and 450 °C (slope: $1.34e^{-4}\pm1.22e^{-5}$, intercept: -0.124 ± 0.00545) which indicate the existence of dissimilar polymers (laminated by PET and PP polymer identified by

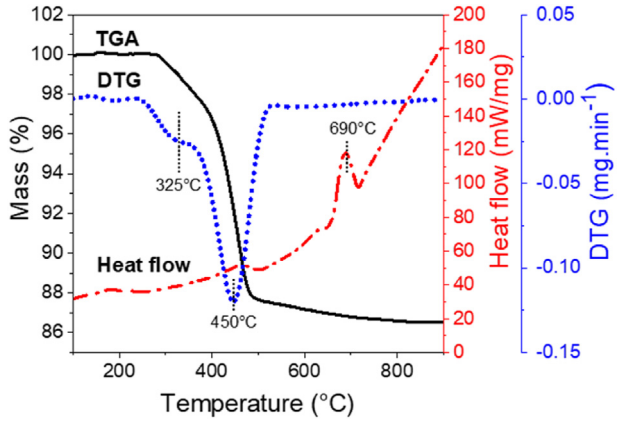

Fig. 3. Thermogravimetric, derivative, and heat flow analysis of the PLAP materials.

the FTIR) in the PLAP materials thermally degrade at two regions from the similar results found by Ng et al. (2018). The heat flow characteristic curve for the process represents two endothermic peaks (at 450 °C and 690 °C), where there is no evidence for any kind of exothermic reactions. The first peak at 450 °C can be ascribed to the sharp decomposition of the PLAP materials due to the devolatilization of the laminated polymers at around this temperature, and the second peak 690 °C has been attributed due to the melting point of the aluminum. It can be noticed that the smelting point temperature in the case of thermal decomposition of the PLAP materials has been slightly increased.

The composition of the aluminum after the thermal disengagement technique (TDT) represented in Table 2 can be estimated by the inductively coupled plasma (ICP) technique. From the analysis, it can be observed that the purity of the aluminum was more than 99%, the rest of the elements are Fe, Si, etc. Along with the metallic components present in the thermally degraded aluminum, carbon content was left behind by the characteristic degradation of the laminated polymers.

Based on the thermogravimetric analysis the thermal degradation temperature of the PLAP materials was selected as 550 °C and the heating time was 20 min to ensure the comprehensive degradation of the laminated polymers into graphitic carbon materials. Fig. 4 represents raw PLAP and the decomposed products (C, Al) found after the thermal disengagement of PLAP materials at 550 °C for 20 min. A layer of carbon particles was detected on the aluminum surface after the TDT which was easily removable by mechanical processing. In this research, carbon particles along with the aluminum foil were used to produce carbon-reinforced aluminum microparticles.

3.2. Qualitative analysis of the synthesized oil

The polymers were devolatilized at 600 °C, the organic matters released from the polymers were condensed and collected for further analysis. The collected oil from the pyrolytic degradation of the laminated polymers on the aluminum film in PLAP materials was analyzed in the GC-MS to determine the chemical components. Multiple compounds were detected by the gas chromatography (Fig. 5) of the dark grey oil. The summary of the elements detected by the GC-MS of the condensed oil has been represented in Fig. 6. The condensed oil contains aromatic hydrocarbons (Xylene- C_8H_{10}, Isopropyl benzene- C_8H_8, Cymol- $C_{10}H_{14}$, Indene- C_9H_8, Naphthalene- $C_{10}H_8$, 5-acetyl indane- $C_{12}H_8$), organic compounds (Styrene- C_8H_{10}, Phenol- C_6H_5OH, Propenol- C_3H_6O, 2-methyl benzofuran- C_9H_8O, 2, 3-dihydro-2-

Table 2
Composition of the aluminum after thermal disengagement.

Components	Al	Fe	Si	K	Cu	Ga	Mg	Ti	Na	Mn	V	P	Zn	Cr	Ni	B	Pb	Sn	Zr	Mo	As	Co	Sb	U
Weight (%)	99.194	0.4515	0.1515	0.0874	0.0204	0.0187	0.0183	0.0121	0.0112	0.0104	0.0074	0.0069	0.0030	0.0021	0.0021	0.0009	0.0006	0.0003	0.0002	0.0002	0.0002	0.0001	0.0001	0.0001

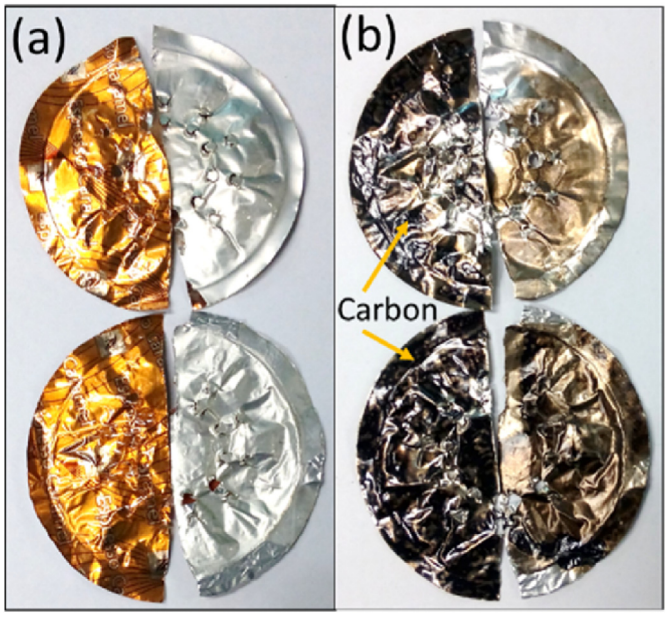

Fig. 4. (a) Raw PLAP, and (b) thermo-disengaged materials at 550 °C (20 min) showing carbonaceous materials on the surface of the aluminum.

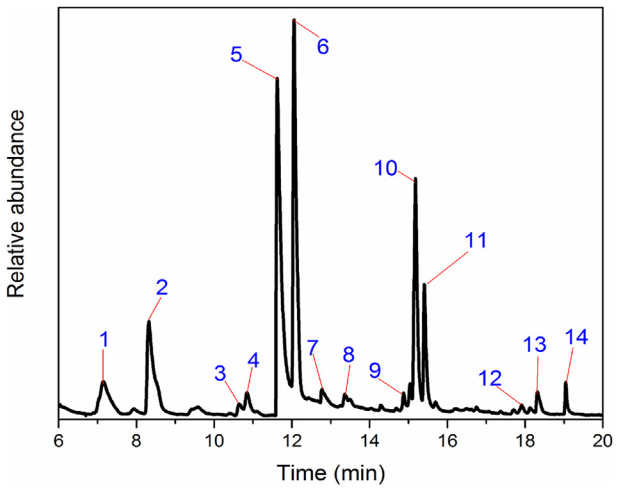

Fig. 5. GC-MS chromatogram of the oil collected from the polymers in the PLAP materials.

methyl benzofuran- $C_9H_{10}O$, 2-Vinyl-2,3-dihydro benzofuran- $C_{10}H_{10}O$) melamine (Benzonitrile- C_7H_5N), and heterocyclic compound (Benzofuran- C_8H_6O). Even though there are many different compounds in the chemistry of the oil, considerably the main component is an aromatic hydrocarbon. It is well known from the literature, the pyrolysis of the polyethylene terephthalate (PET) in the N_2 atmosphere above 600 °C can produce aromatic hydrocarbons (Dziwiński et al., 2018; Samperi et al., 2004). So, it can be assumed that the aromatic group of hydrocarbons in the condensed oil comes from the degradation of the PET, and some other scattered hydrocarbon chain elements might be attributed by the pyrolytic decomposition of the polypropylene and some sort of other materials like resign, paints etc.

3.3. Morphology and particle size distribution

Fig. 7(a–b) represent the morphology of the aluminum powders fabricated by the cryo-milling of 2 and 4 cryogenic cycles. Though cryo-milling for 2 cycles can produce some powders, most of them remain larger in size, which can be easily understood by physical and microscopic observation. From Fig. 7 (a), it can be observed that the raw aluminum sample started to become flat and due to the impact of the ball at a low temperature, some flake shaped aluminum tore off from the cluster. A significant change occurs after running the cryo-mill for four cycles. The large chunk of the metal has been destroyed by fracturing the surface of the bulk material. When several fresh fracture surfaces come together by the impact of the ball and compressed with the wall of the grinding chamber, they form a bonding between two fresh surfaces and cold-welded together. This cold-welded cluster again absorbs friction and impact energy and initiate the crack, the propagation of the crack again causes fracture of the particles. Initially, the particles agglomerate quickly and after running for a few minutes at extremely low temperature the plastic deformation dominates, and particle size becomes smaller.

At lower temperature the brittleness of the metal increases that leads to the reduction of ductility and due to the work hardening the surface hardness also increases. Therefore, an improved tendency of the particles to be fractured has been observed after the initial stage where cold welding happens more often rather than the fracturing tendency. In the second stage of the cryo-milling crack initiation and deformation leads to fracture happens more readily than cold welding as a result the size of the particles reduces continuously from the second stage of cryo-milling though the shape and size of the particles changing always depend on the brittleness, hardness, stress, and strain developed, impact and friction of the grinding ball and jar. In the last stage of the grinding, the process becomes a quite steady state, where there is a good balance between the cold welding and fracture behavior and thus the average particle size of the material does not change rapidly (Enayati, 2017).

Fig. 7 (c & d) represent the morphology of the cryo-milled powder after running the mill for 6 and 8 cycles. Though the agglomeration of the particles dominates after 4 cycles of cryo-milling, after running the process for 6 cycles or more the fracture behavior leads the agglomeration and a significant reduction of the particle size has been observed from the corresponding images. SEM images of the cryo-milled powders represent the shape, size, and morphology of the particles where the minutest variation can be observed between the powders received from 6 to 8 cycles. Moreover, some free particles can also be identified along with the agglomerates formed by pressing the smaller particles together. As the variation in particle size between the last two processing conditions is insignificant, therefore, it can be estimated as the optimum conditions for the cryo-milling parameters.

Fig. 8 represents the particle size distribution of aluminum powders produced by different milling times using cryo-mill in a cryogenic condition. The cryo-mill starts production of powder while it runs for at least 4 cycles (29 min) and the change in shape and size is significant compared to the output from less milling time. The average size of the particles is 123 μm, 71 μm, 64 μm, and 38 μm found after running the cryo-mill for 2, 4, 6, and 8 cycles respectively. The size of 68% of the particles is below 50 μm for 6 cycles cryo-milling where this percentage is 83% for the particles produced by 8 cryo-milling cycles. About 55% of the particles are below 25 μm in size found from the last stage of the milling (8 cycles, 53 min). Initially, the materials ductile behavior changes and fractures begin to produce small particles but due to the agglomeration of the particles they form a cluster and this behavior is strongly dominating up to 6 cycles of running the cryo-mill. After 6 cycles the agglomeration and fracture behavior reach an equilibrium condition. So, particle size reduction after 6 cycles become

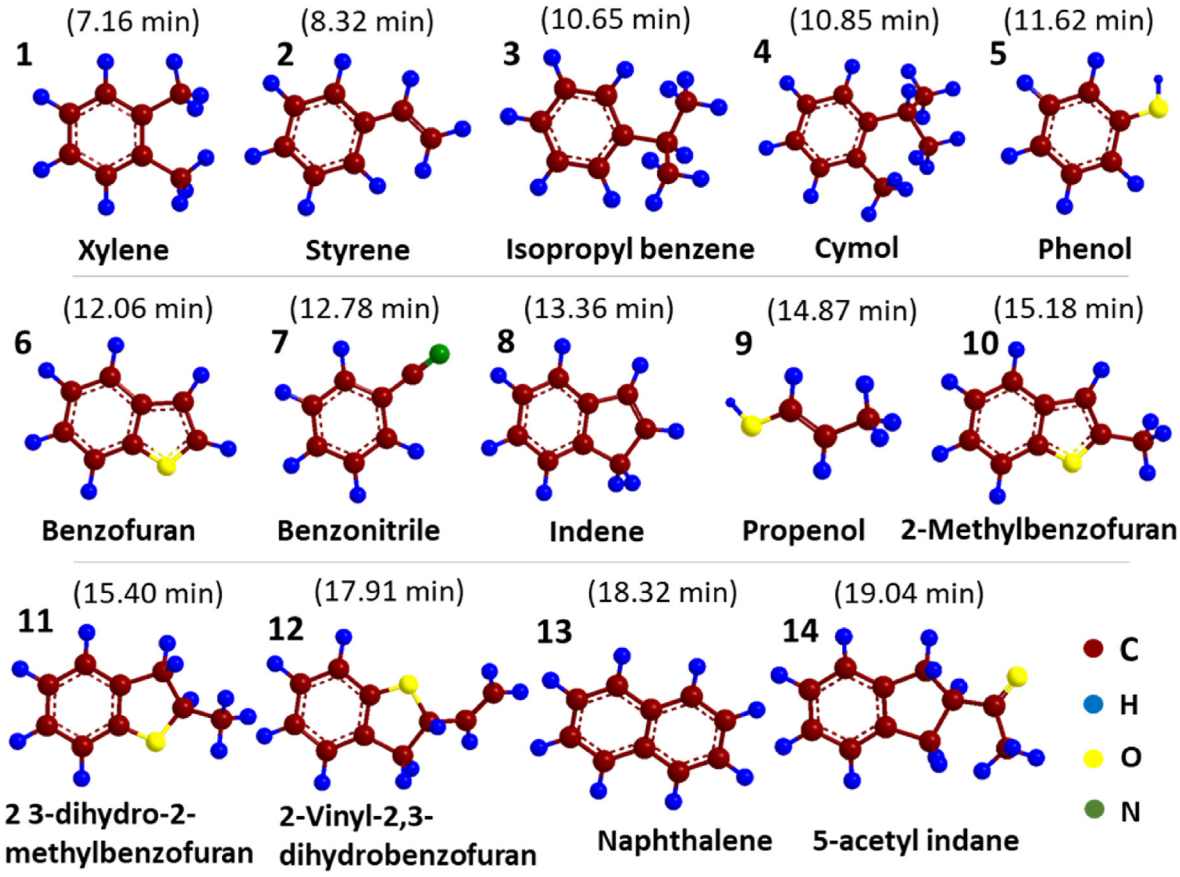

Fig. 6. Identified chemical elements in the condense oil.

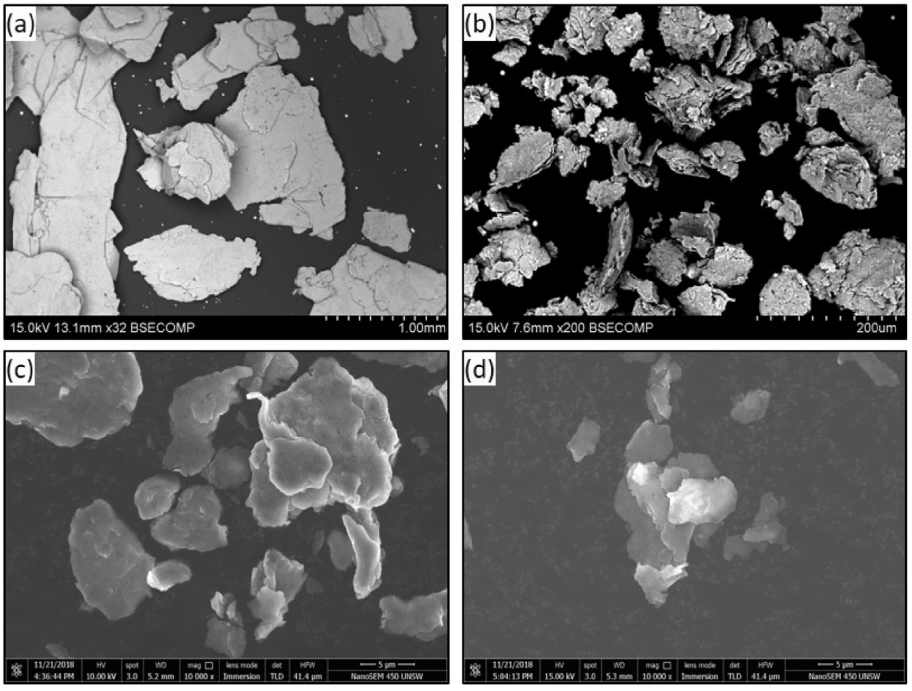

Fig. 7. SEM images of the aluminum powders after different cycles of cryo-milling (a) 2 cycles, (b) 4 cycles, (c) 6 cycles, and (d) 8 cycles.

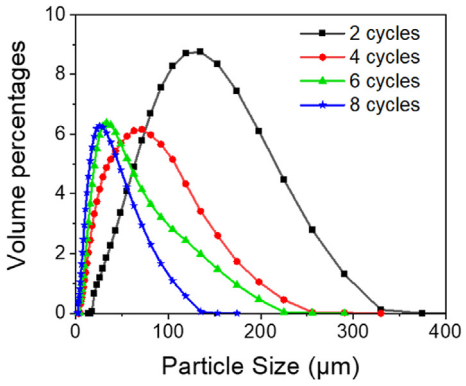

Fig. 8. Particle size distribution.

insignificant and a narrow particle size distribution found below the particle size of 50 μm. Even though there is a lack of uniformity in the particle size distribution of the Al microparticles in the low milling cycles, it can be significantly improved by increasing the cryo-milling time. Moreover, the particles fabricated by this method can be utilized in the field of applications where the uniformity of the particles size and shapes are less important, for example pyrolytic displaying components, paints, burning fuel etc.

3.4. Structural analysis

Thermo-disengaged aluminum was cryo-milled for the different time periods with the different cryogenic cycles (2, 4, 6, and 8) in a liquid nitrogen-cooled atmosphere without the direct contact with any coolant or additives. Fig. 9 (a) represents the comparison of X-ray diffraction patterns for four different types of aluminum powders produced by the cryo-milling process. The peaks are quite consistent and similar in terms of positions (at 38.48° (111), 44.73° (002), 65.11° (022), 78.24° (113), and 82.45° (222)) and they are confirmed as the reflection by face-centered cubic (FCC) aluminum (lattice parameters: 4.0490). No other major peaks are indexed in the representation though there might have some oxidation of the powder aluminum and there is a possibility to form Al_2O_3. The oxidation of the synthesized Al microparticles was minimized by the controlling the unloading of the particles from the cryo-mill. It was left for a few hours to balance the temperature of the Al with the ambient temperature to avoid the thermal shock while it opens to the environment. Rufino et al. explained that if a very thin layer of the amorphous oxide layer formed on the aluminum powder, it is very hard to detect by the X-ray diffractometry (Rufino et al., 2007). In addition, there is a small percentage of carbon particles introduced in the aluminum microparticles by the scission decomposition of the laminated polymers, which was also undetectable by the XRD due to its lower concentration.

Though the XRD patterns of cryo-milled powders have shown almost similar characteristics, there are some specific differences among the individual patterns represented in Fig. 9 (b). The reduction of peak intensity and the peak broadening phenomena have been observed with the change of milling time of the aluminum powder. The effect of milling time, particle size and microstrain developed in particles are the root causes of this peak broadening (Kumar and Biswas, 2017). The aluminum becomes fine powder while the cryo-mill runs for at least 4 cycles observed from the scanning electron microscopy and particle size distribution. The drastic change in the peak intensity observed after the diffraction of 2 cycles cryo-milling aluminum powders and it also indicates some significant changes in the particle size and structure of the powders. Though almost similar intensities of the peaks have been found from the diffraction patterns of aluminum powders found from 4 to 6 cryogenic cycles, there is a noticeable peak broadening and this peak broadening is maximum for the XRD pattern of 8 cycles cryo-milled aluminum powder.

Fig. 10 represents the change in crystallite size and the percentages of microstrain developed during the low-temperature cryo-milling process of aluminum powder production. The crystallite size and microstrain of the powder particles have been estimated by Rietveld fit. Both the crystallite size variation and microstrain variation are monotonic over the time period of high energy cryo-milling where initially a rapidly changing behavior of the micro-strain has been observed. When the materials are milled for a higher time period, the behavior of the micro-strain changing is insignificant where in case of crystallite size, it shows a slight change in the initial milling conditions and completely opposite after running the cryo-mill for 6 continuous cycles and the minimum crystallite size (476 Å) has been observed for the aluminum powders produced by 8 cryo-cycles millings. In this condition, the percentage of micro-strain developed is highest (0.18). The initial increment of the microstrain is due to the deformation without any permanent fracture of the bulk material caused by the impact of the high energy movement of grinding ball. At this time, embrittlement of the materials and cold welding of the smaller particles already formed by the low-temperature milling which can also make an addition to the micro-strain. After several cycles of cryo-milling, the plastic deformation of the grain boundaries leads the agglomeration and cold-welding phenomena. Thus, the behavior of the percentage change of strain becomes persistent. Larger crystallites initially absorb the impact and friction energy and when the microstrain level reaches a critical point, it starts to develop a fracture in the grain boundaries (Hellstern et al., 1989; Trudeau et al., 1992). The size reduction of the crystallites can be caused by the partial formation of the grain boundary deformation, movement of the dislocation from the boundary to the other

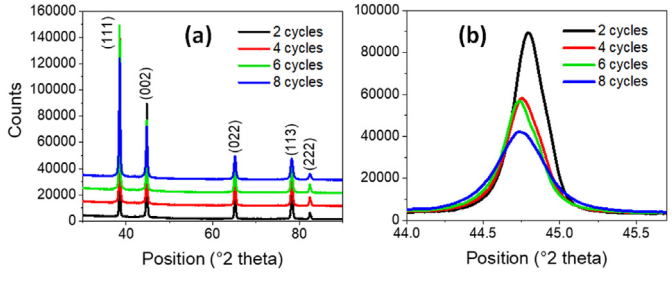

Fig. 9. (a) Comparison of the XRD pattern (Reference code: 98-006-4700) for aluminum powders with different cryo-milling time and (b) Magnified representation of the peaks showing peak broadening.

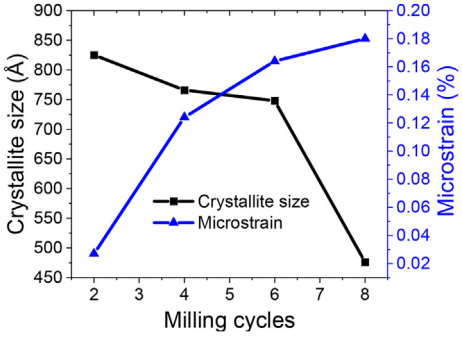

Fig. 10. Variation of crystallite sizes and strain percentages with milling cycles.

regions of the grains and formation of the irregular fracture in the cluster of grains (Gómez et al., 2006).

3.5. X-ray photoelectron spectroscopy (XPS)

The surface of the cryo-milled aluminum microparticles was analyzed by the X-ray photoelectron spectrometer with depth profile and elemental imaging which is a very sensitive instrument for the analysis of a few outermost atomic layers with a sampling depth approximately 1–10 nm (Tougaard, 2010). Fig. 11 represents the estimation of aluminum, Oxygen, and Carbon present on the surface of the fabricated aluminum powder. Fig. 11 (a) represents the overall survey scan of the XPS analysis and Fig. 11 (b) represents the spectra for Al2p peaks at 75.27 eV, 72.13 eV, 79.75 eV, and 77.93 eV which can be identified as Al_2O_3/Al (Asadabad and Eskandari, 2016), Al (Liu et al., 2013), Al_2O_3 (Lindsay et al., 1973), and AlO(OH) (Lindsay et al., 1973) for the corresponding binding energy from the National Institute of Standard and Technology (NIST) database. Similarly, from Fig. 11(c–d) the peaks for C1s (284.8 eV, 286.3 eV, 287.8 eV, 288.8 eV, and 290.17 eV) and O1s (532.04 eV, 534.85 eV, and 536.97 eV) can be identified as C (Bachman and Vasile, 1989), –C(O)- (Lopez et al., 1986), C≡C (Ocal and Ferrer, 1986), $(CO)_6$ (Gelius et al., 1970), $(CO)_2$ (Onishi et al., 1987) and Al_2O_3 (Dua et al., 1988), SiO_2 (Dua et al., 1988), O_2/C (Tillborg et al., 1993). The atomic percentage of aluminum (Al-(Al2p)), oxygen (O-(O1s)), and carbon (C-(C1s)) on the outermost atomic layers of the fabricated aluminum powder was estimated as 37.06%, 59.77%, and 2.4%. A small trace of silicon was also detected by the XPS, which might be derived from the alloying elements of the raw aluminum used to make the foil. The oxygen concentration on Al surface comes from its oxide component (Al_2O_3), atmospheric air adsorption, and slightly from the composition of SiO_2. The main reason for the oxygen trace found on the aluminum powders surface is due to the oxidation behavior of the aluminum powder at any temperatures (Liu et al., 2017; Hasani et al., 2012; Kovacich and Lichtman, 1985; Kowalski et al., 1992). The presence of organic substances with the waste coffee capsules consequences the existence of free carbon and hydrocarbons in the heated capsules and finally, the traces of those organic substances may be found in the final cryo-milled aluminum powder (Yin et al., 2019b). The samples were exposed to the atmospheric air for about 4 weeks before doing the XPS analysis, thus the existence of oxygen might be engaged from the atmosphere (Kumar and Biswas, 2017).

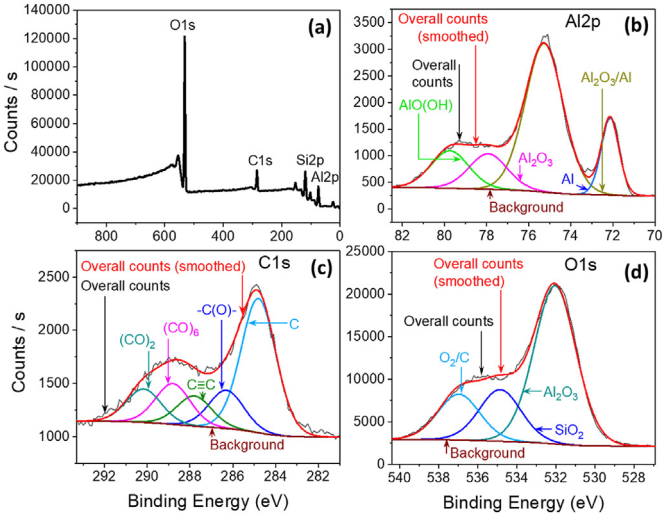

Fig. 11. X-ray photoelectron spectroscopy spectra of cryo-milled aluminum powder: (a) overall survey, (b) Al2p, (c) C1s, and (d) O1s.

3.6. Thermal properties

Thermogravimetric (TGA) analysis of the aluminum powders of different particle sizes has represented in Fig. 12. Thermal behavior of the powders received from 2 cycles cryo-milling is quite different from other powders found from 4, 6, and 8 cryo-milling cycles. Initially, there is a slight weight loss for all categories due to the evaporation of moisture content and adsorbed gases from the fabricated powders (Sarathi et al., 2007; Nazarenko et al., 2014). This initial loss of weight depends on the amount of moisture present in the storage facility, reaction chamber of TGA, and quality of the nitrogen gas supplied to the chamber. With the increasing temperature beyond 500 °C, all the powders except the first one (2 cycles) start to gain weight by reacting with atmospheric oxygen still present with the supplied nitrogen gas and forming aluminum oxides on the surface of the powders. While the temperature reaches the melting point, the rate of oxidation accelerates for all fine aluminum powders (Vorozhtsov et al., 2016). Paravan et al. suggested that the finer particles have more surface area and thus the oxidation for finer particles is higher in comparison to the large particles (Paravan et al., 2018). Similarly, our study shows a higher oxidation behavior for the smaller particles found from the more milling time.

Heat flow characteristics of the fabricated aluminum powders have been illustrated by Fig. 13(a–b). All powders have shown endothermic behavior at close to the melting point temperature of aluminum. But there is a slight difference between the powders of different particles sizes fabricated by different cryo-milling cycles. With the increasing milling time, the particles become finer in size and shape and thus the heat flow increases for finer particles compared to the other powders with larger particle sizes found from less milling time period. From Fig. 13 (a), it can be observed that the heat flow increases from 7.02 mW/mg (at 658 °C for 2 cycles powder) to 10.54 mW/mg (at 663 °C for 8 cycles powder). For the improvement of heat flow, the melting point of smaller particles goes down which is also describable from Fig. 13 (b), the derivative curves for the heat flow of different aluminum powders. Generally, two types of peaks (Exothermic and Endothermic) can be observed if the aluminum powders are heated in air or any other oxidation media (Arockiasamy et al., 2009). Nitrogen is the most commonly used media where some people used argon, hydrogen or even vacuum (Jha et al., 1988; Schaffer et al., 2006; Kondoh et al., 2001; Martın and Castro, 2003; Schaffer and Hall, 2002). From Fig. 13 (a), only endothermic peaks are observed for all powders due to the melting of aluminum where there are no exothermic peaks due to the minor oxidation happens as the environment in the

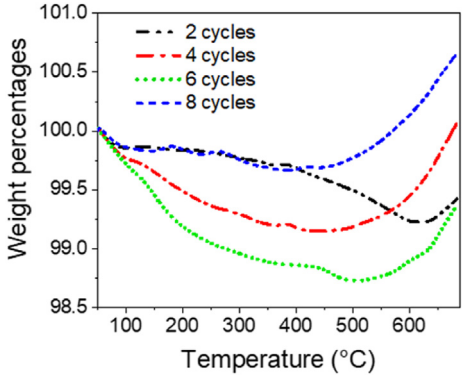

Fig. 12. Thermogravimetric analysis of fabricated aluminum powders.

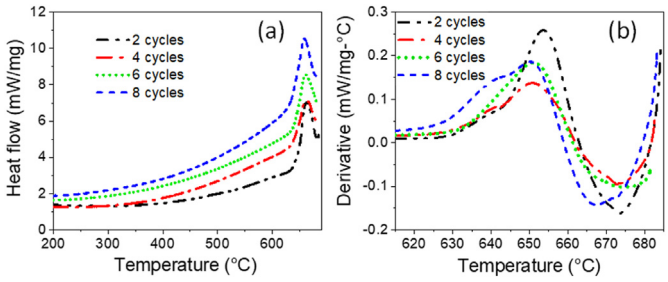

Fig. 13. (a) Heat flow characteristics and b) derivative of the heat flow for the fabricated aluminum powders.

reaction chamber was inert (Liu et al., 2017; Rufino et al., 2010).

3.7. Dispersibility

Dispersion of the aluminum particles is an important property to understand the ability to mix with other media during the fabrication of paint and other industrial products. It is also useful to measure the particle size and the ability of the particles to move freely (Lu et al., 2005). The dispersion ability of the fabricated aluminum microparticles has been illustrated in Fig. 14. Fig. 14 (a) represents the sedimentation of the aluminum microparticles in ethanol, methanol, acetone, propanol, and water. Where, Fig. 14 (b) represents the dispersion of the aluminum microparticles in the same media after sonication. Fig. 14 (c & d) are the sedimentation and dispersion of aluminum microparticles in the same media after 60 days. From the experiment, it has been observed that the aluminum microparticles can be sedimented in the liquids except for water within 4 h. Fabricated powders can move freely in the solvents without any kind of agglomerations. An exothermic reaction takes place when the aluminum microparticles are mixed with water (Urbonavicius et al., 2017). Thus, the aluminum microparticles cannot be properly mixed with water due to that obvious reaction phenomenon where there are no such reactions with the other liquids, and this is the evidence of high dispersibility of fabricated aluminum microparticles without agglomeration.

3.8. Transmission Electron Microscopy

Fig. 15(a–d) represent the bright field Transmission Electron Microscopy (TEM) images of the aluminum powders fabricated by 2, 4, 6, and 8 cryogenic milling cycles. Aggregates of the particles can be observed from the bright field images, where several layers of the powder particles agglomerate together before they formed into fine particles by absorbing friction and grinding impacts. Microparticles are seen with sharp edges and clear boundaries which indicate the possibility to form nanoparticles upon further processing of the particles fabricated by this process. Fig. 15 (e) represents the corresponding selected area electron diffraction (SAED) pattern of the fabricated aluminum microparticles where the crystallographic planes are identified as 111, 002, 022, 113, and 222 which is identical with the planes identified from x-ray diffraction shown in Fig. 9. Clear rings with white dots of the pattern indicate the polycrystalline face-centered cubic (FCC) structure of the aluminum microparticles (Asadabad and Eskandari, 2016).

4. Technical cost analysis

Cost estimation for the operation of a cryo-mill is important to explore the feasibility of the process to utilize in commercial applications. Moreover, it has great importance in materials selection, selection of the process technology, product design, etc. The cost analysis of mechanical processing and product manufacturing depends on many variables and fixed elements. The variable cost elements for running a cryo-mill is enlisted in Table 3, where the fixed costs, for examples machine purchase cost, depreciation cost, tool cost, installation cost, maintenance cost, auxiliary component

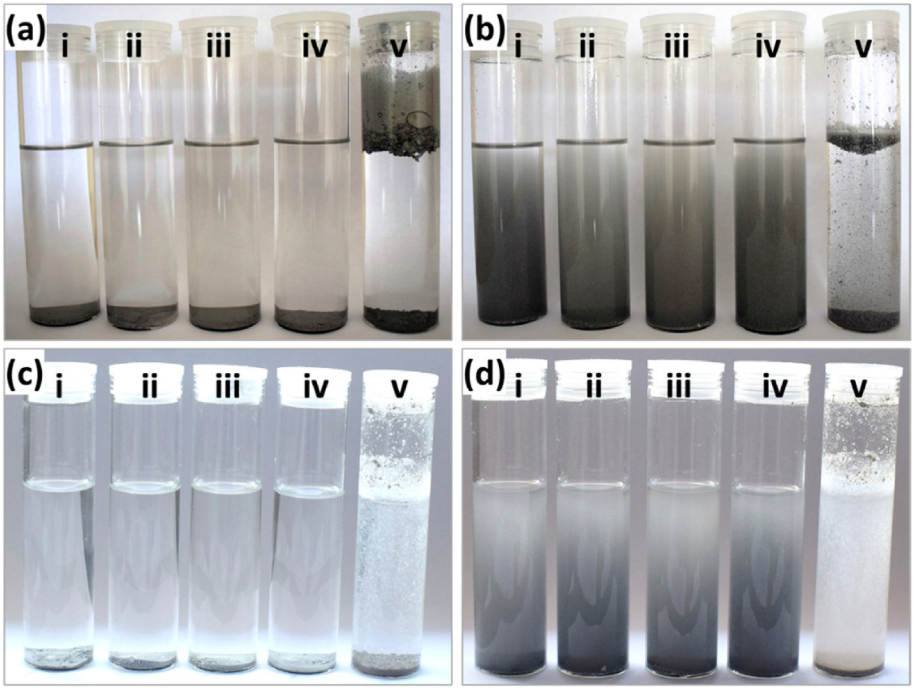

Fig. 14. Dispersibility: (a) sedimentation of aluminum microparticles in (i) ethanol, (ii) methanol, (iii) acetone, (iv) propanol, and (v) water, (b) dispersion in same media, and (c, d) sedimentation and dispersion after 60 days.

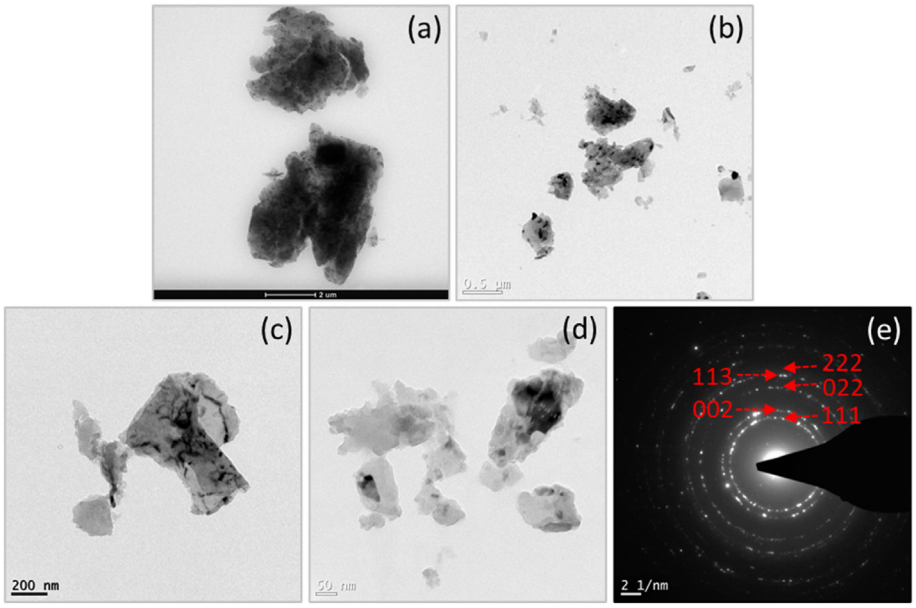

Fig. 15. Bright-field TEM images for aluminum powders made by cryo-milling for (a) 2 cycles, (b) 4 cycles, (c) 6 cycles, (d) 8 cycles, and (e) selected area electron diffraction image.

Table 3
Variable cost elements for cryo-milling.

Variable cost components	Cost (A$)
Labor cost (operating the cryo-mill)	19.49 A$/h
Liquid N_2 cost	0.75 A$/L
Utility: Electricity	0.34/kWh
[a]Safety and cleaning	–
[b]Materials collection, and preprocessing cost	–

[a] No cost included as the operator can perform simultaneously.
[b] Raw materials collected from the local facilities without any cost.

cost, overhead labor cost, and building costs are excluded from the calculations in this study. In this research, it can be observed that the thin aluminum was converted into microparticles within 41 min. To make the calculation in a safe limit we have considered the operation time is 1h. The labor cost according to the Australian national employment standard is a minimum 19.49 A$ per hour (Commonwealth of Australia, 2019). The consumption of liquid nitrogen is an important factor in cost estimation. It has calculated based on the recorded data in the laboratory and the empirical formula proposed by Peters et al. as bellow (Peters et al., 2003):

$$R = r\left(\frac{Q}{q}\right)^{0.8} \quad (1)$$

Where, R = Commercial-scale N_2 consumption rate, r = N_2 consumption rate in laboratory scale, Q = The capacity in commercial scale, and q = Laboratory-scale production capacity. The concept for the capacity scaling was introduced with the exponent value 0.8, which was rationalized by the intentional variation in the known capacity in the laboratory scale (Ye and Schoenung, 2004). The cost of electricity is comparatively lower, and it has been assumed that there is a minor change in the electric cost with the scaling up the process to a higher capacity. The cost for raw materials collection and cleaning the equipment is excluded as it was negligible in the laboratory scale and very much unpredictable for the industrial scale.

Fig. 16 represents the cost of Al microparticles per Kg of production. The cost of the production exponentially decreases with

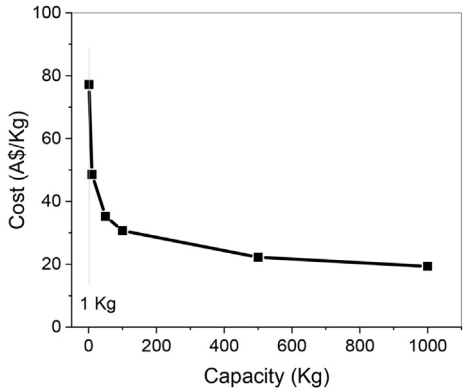

Fig. 16. Cost of aluminum microparticles per Kg with the variation of the processing capacity.

the increasing of the processing capacity and finally when the processing capacity is 1000 Kg, the processing cost is 19.35A$/Kg. A brief analysis of the costing might be interesting for the investment in the industrial-scale production of Al microparticles in a non-conventional low-temperature milling process described in this research. The major cost in this analysis attributed to the consumption of liquid N_2 (~90% of the variable cost, in lab-scale production). In the laboratory-scale processing the yield of Al microparticles is quite low, only 10 g (LN_2 consumption 3 L/h). But in the real case, in the industrial applications, the cost will be significantly reduced as there will be mass-produced in a single run. Ye et al. investigated the cost of cryo-milling on an industrial scale and they found that the liquid N_2 can contribute 27% of the total cost (Ye and Schoenung, 2004).

5. Conclusions and future prospects

Polymer laminated thin aluminum packaging waste was transformed into solid Al, graphitic carbon, bio-oil, and finally Al microparticles in this study. The conclusions can be drawn as:

1. The thermal disengagement at 550 °C for 20 min recycled the PLAP materials into solid Al and graphitic carbon particles.
2. When the PLAP materials were thermally disengaged in gaseous N_2 atmosphere at 600 °C for 1h, the laminated polymers degraded into bio-oil.
3. Aluminum microparticles were fabricated by cryo-milling the thermo-disengaged PLAP materials (at 550 °C) where the particle size below 100 μm was achieved within 30 min of the milling period.
4. Aluminum powders produced from the cryo-milling process are flake shaped with a large surface area. A small percentage of carbon materials were detected in the aluminum microparticles which might be very useful for additive manufacturing.
5. There was an insignificant variation observed in the particle size, crystallite size, and micro-strain development after the cryo-milling for 6 cycles. Therefore, optimization of the milling parameters can be achieved at 6 cycles (41 min).
6. With the reduction of the particle size of the fabricated aluminum powder, an improvement of the thermal stability and the heat flow characteristics was observed.
7. Aluminum microparticles have shown good dispersibility behavior in polar liquids without any kind of agglomeration.

Future analysis: This research has explored a pathway to fabricate microparticles from the waste packaging materials. In addition, the bio-oil synthesis capability from the polymer laminates has also been primarily analyzed. More analysis in future required to synthesis the nanoparticles of the ductile metal (Al) by non-traditional technique like cryo-milling. A brief analysis on the prospect of bio-oil synthesis from the waste packaging material can be an important option for future research. The milling process in cryogenic temperature can be extended to the industrial scale upon further research on the design considerations of the process technology and upscaling feasibilities.

Declaration of competing interest

The authors declare that they have no known competing financial interests or personal relationships that could have appeared to influence the work reported in this paper.

CRediT authorship contribution statement

Abdullah Al Mahmood: Writing - original draft, Writing - review & editing, Formal analysis, Investigation, Methodology, Visualization. **Rumana Hossain:** Supervision, Writing - original draft, Writing - review & editing, Formal analysis, Investigation, Methodology, Visualization, Conceptualization, Validation. **Saroj Bhattacharyya:** Formal analysis, Visualization. **Veena Sahajwalla:** Funding acquisition, Project administration, Supervision, Conceptualization, Formal analysis, Validation, Resources, Writing - review & editing.

Acknowledgments

This research was supported by the Australian Research Council's industrial transformation research hub funding scheme (project: IH130200025). We gratefully acknowledge Dr. Irshad Mansuri and the technical and analytical support given by the Mark Wainwright Analytical Centre (MWAC), UNSW, Sydney, Australia.

References

Al Mahmood, A., Hossain, R., Sahajwalla, V., 2019. Microrecycling of the metal−polymer-laminated packaging materials via thermal disengagement technology. SN Appl. Sci. 1, 1. https://doi.org/10.1007/s42452-019-1099-7.
Arockiasamy, A., German, R., Wang, P., Horstemeyer, M., Suri, P., Park, S., 2009. DSC analysis of Al6061 aluminum alloy powder by rapid solidification: effect of additives. J. Therm. Anal. Calorim. 100, 361−366.
Asadabad, M.A., Eskandari, M.J., 2016. Electron diffraction. In: Mod. Electron Microsc. Phys. Life Sci., IntechOpen.
Bachman, B.J., Vasile, M.J., 1989. Ion bombardment of polyimide films. J. Vac. Sci. Technol. A Vacuum, Surfaces, Film. 7, 2709−2716.
Blackburn, P.E., Gulbransen, E.A., 1960. Aluminum reactions with water vapor, dry oxygen, moist oxygen, and moist hydrogen between 500° and 625° C. J. Electrochem. Soc. 107, 944−950.
Commonwealth of Australia, 2019. Employees pay, leave and entitlements. n.d. https://www.business.gov.au/People/Pay-and-conditions/Employees-pay-leave-and-entitlements. accessed April 14, 2020.
Cox, A.R., Tillman, T.D., Patterson, R.J., 1978. Application of rapidly solidified alloys. PRATT AND WHITNEY AIRCRAFT GROUP WEST PALM BEACH FL GOVERNMENT PRODUCTS DIV.
Dua, A.K., George, V.C., Agarwala, R.P., 1988. Characterization and microhardness measurement of electron-beam-evaporated alumina coatings. Thin Solid Films 165, 163−172.
Dziwiński, E.J., Iłowska, J., Gniady, J., 2018. Py-GC/MS analyses of poly(ethylene terephthalate) film without and with the presence of tetramethylammonium acetate reagent. Comparative study, Polym. Test. 65, 111−115. https://doi.org/10.1016/j.polymertesting.2017.11.009.
Enayati, M.H., 2017. Nanocrystallization of Al powder by cryomilling process. KONA Powder Part. J. 2017, 207−212. https://doi.org/10.14356/kona.2017006.
Gelius, U., Hed, P.F., n, Hedman, J., Lindberg, B.J., Manne, R., Nordberg, R., Nordling, C., Siegbahn, K., 1970. Phys. Scripta 2, 70.
Gómez, B., Gordo, E., Torralba, J.M., 2006. Influence of milling time on the processing of Fe−TiCN composites. Mater. Sci. Eng. 430, 59−63.
Groza, J.R., 1999. Sintering of nanocrystalline powders. Int. J. Powder Metall. 35, 59−66. Princeton, New Jersey. https://www.scopus.com/inward/record.uri?eid=2-s2.0-0033347838&partnerID=40&md5=30a379b48e7b57fe6d643e9b59a06b05.
Guo, L., Song, W., Hu, M., Xie, C., Chen, X., 2008. Preparation and reactivity of aluminum nanopowders coated by hydroxyl-terminated polybutadiene (HTPB). Appl. Surf. Sci. 254, 2413−2417. https://doi.org/10.1016/j.apsusc.2007.09.043.
Gutmanas, E.Y., Trusov, L.I., Gotman, I., 1994. Consolidation, microstructure and mechanical properties of nanocrystalline metal powders. Nanostruct. Mater. 4, 893−901. https://doi.org/10.1016/0965-9773(94)90095-7.
Haber, J.A., Buhro, W.E., 1998. Kinetic instability of nanocrystalline aluminum prepared by chemical synthesis; facile room-temperature grain growth. J. Am. Chem. Soc. 120, 10847−10855. https://doi.org/10.1021/ja981972y.
Hasani, S., Panjepour, M., Shamanian, M., 2012. The oxidation mechanism of pure aluminum powder particles. Oxid. Metals 78, 179−195.
He, J., Chung, K.H., Lavernia, E.J., Liao, X., Zhu, Y.T., 2003. Mechanical milling-induced deformation twinning in Fcc materials with high stacking fault energy. Metall. Mater. Trans. 34, 707−712. https://link.springer.com/article/10.1007/s11661-003-0106-0.
Hellstern, E., Fecht, H.J., Fu, Z., Johnson, W.L., 1989. Structural and thermodynamic properties of heavily mechanically deformed Ru and AlRu. J. Appl. Phys. 65, 305−310.
Hull, M., 2002. Tetronics: plasma processing holds key to consistent nanopowders. Powder Metall. 45, 8−9. https://doi.org/10.1179/pom.2002.45.1.8.
Jha, A.K., Prasad, S.V., Upadhyaya, G.S., 1988. Effect of sintering atmosphere and alumina addition on properties of 6061 aluminium P/M alloy. Powder Metall. Int. 20, 18−20.
Karthik, P.S., Chandrasekhar, S.B., Chakravarty, D., Srinivas, P.V.V., Chakravadhanula, V.S.K., Rao, T.N., 2018. Propellant grade ultrafine aluminum powder by RF induction plasma. Adv. Powder Technol. 29, 804−812. https://doi.org/10.1016/j.apt.2017.12.024.
Khan, A.S., Farrokh, B., Takacs, L., 2008. Effect of grain refinement on mechanical properties of ball-milled bulk aluminum. Mater. Sci. Eng. 489, 77−84. https://doi.org/10.1016/j.msea.2008.01.045.
Koch, C.C., 1989. Materials synthesis by mechanical alloying. Annu. Rev. Mater. Sci. 19, 121−143.
Kondoh, K., Kimura, A., Watanabe, R., 2001. Effect of Mg on sintering phenomenon of aluminium alloy powder particle. Powder Metall. 44, 161−164.
Kovacich, J.A., Lichtman, D., 1985. A qualitative and quantitative study of the oxides of aluminum and silicon using AES and XPS. J. Electron. Spectrosc. Relat. Phenom. 35, 7−18. https://doi.org/10.1016/0368-2048(85)80038-4.
Kowalski, L., Korevaar, B.M., Duszczyk, J., 1992. Some new aspects of the theory of oxidation and degassing of aluminium-based alloy powders. J. Mater. Sci. 27, 2770−2780. https://doi.org/10.1007/BF00540704.
Kumar, N., Biswas, K., 2017. Cryomilling: an environment friendly approach of preparation large quantity ultra refined pure aluminium nanoparticles. J. Mater. Res. Technol. 1−12. https://doi.org/10.1016/j.jmrt.2017.05.017.
Kwon, Y.-S., Jung, Y.-H., Yavorovsky, N.A., Illyn, A.P., Kim, J.-S., 2001. Ultra-fine powder by wire explosion method. Scripta Mater. 44, 2247−2251. https://doi.org/10.1016/S1359-6462(01)00757-6.
Lindsay, J.R., Rose, H.J., Swartz, W.E., Watts, P.H., Rayburn, K.A., 1973. X-ray photoelectron spectra of aluminum oxides: structural effects on the "chemical shift. Appl. Spectrosc. 27, 1−5. https://www.osapublishing.org/as/abstract.cfm?URI=as-27-1-1.
Liu, X., Feng, C., Or, S.W., Jin, C., Xiao, F., Xia, A., Li, W., Sun, Y., Zhao, S., 2013.

Synthesis and electromagnetic properties of Al/AlOx-coated Ni nanocapsules. Mater. Res. Bull. 48, 3887–3891.
Liu, Y., Ren, H., Jiao, Q.J., 2017. Oxidation mechanism of micron-sized aluminum particles in Al-CO2 gradually heating system. In: IOP Conf. Ser. Mater. Sci. Eng. IOP Publishing, p. 12002.
Lopez, L.C., Dwight, D.W., Polk, M.B., 1986. The PI-] PI-star shake-up phenomena IN polyesters containing backbone aromatic-groups. Surf. Interface Anal. 9, 405–409.
Lu, S., Pugh, R.J., T.-S, E.B., 2005. Chapter 10 Dispersion of particles in liquids. In: Forssberg, I.S. (Ed.), Interfacial Sep. Part. Elsevier, pp. 517–558. https://doi.org/10.1016/S1383-7303(05)80011-0.
Mandilas, C., Daskalos, E., Karagiannakis, G., Konstandopoulos, A.G., 2013. Synthesis of aluminium nanoparticles by arc plasma spray under atmospheric pressure. Mater. Sci. Eng. B 178, 22–30. https://doi.org/10.1016/j.mseb.2012.10.004.
Martın, J.M., Castro, F., 2003. Liquid phase sintering of P/M aluminium alloys: effect of processing conditions. J. Mater. Process. Technol. 143, 814–821.
Nazarenko, O.B., Amelkovich, Y.A., Sechin, A.I., 2014. Characterization of aluminum nanopowders after long-term storage. Appl. Surf. Sci. 321, 475–480. https://doi.org/10.1016/j.apsusc.2014.10.034.
Ng, H.M., Saidi, N.M., Omar, F.S., Ramesh, K., Ramesh, S., Bashir, S., 2018. Thermogravimetric analysis of polymers. Encycl. Polym. Sci. Technol. https://doi.org/10.1002/0471440264.pst667.
Ocal, C., Ferrer, S., 1986. The strong metal–support interaction (SMSI) in Pt–TiO2 model catalysts. A new CO adsorption state on Pt–Ti atoms. J. Chem. Phys. 84, 6474–6478. https://doi.org/10.1063/1.450743.
Onishi, H., Egawa, C., Aruga, T., Iwasawa, Y., 1987. Adsorption of Na atoms and oxygen-containing molecules on MgO (100) and (111) surfaces. Surf. Sci. 191, 479–491. https://doi.org/10.1016/S0039-6028(87)81192-5.
Pant, A., Seth, T., Raut, V.B., Gajbhiye, V.P., Newale, S.P., Nandi, A.K., Prasanth, H., Pandey, R.K., 2016. Preparation of nano aluminium powder (NAP) using a thermal plasma: process development and characterization. Cent. Eur. J. Energ. Mater. 13, 53–71. https://doi.org/10.22211/cejem/64964.
Paravan, C., Verga, A., Maggi, F., Galfetti, L., 2018. Accelerated ageing of micron- and nano-sized aluminum powders: metal content, composition and non-isothermal oxidation reactivity. Acta Astronaut. https://doi.org/10.1016/j.actaastro.2018.08.001.
Peters, M.S., Timmerhaus, K.D., West, R.E., 2003. Analysis of cost estimation. Plant Des. Econ. Chem. Eng. 226–275.
P.M. Research, 2018. Aluminium powder market. https://globenewswire.com/news-release/2018/03/14/1422109/0/en/Aluminium-Powder-Market-to-Exceed-USD-3bn-by-2025-Growing-at-a-CAGR-3-4-between-2017-and-2025-Says-Prof-share-Market-Research.html accessed December 10, 2018.
Primary Information Services, 2018. Aluminum powder production and properties, technology, applications, patent, consultants, company profiles, reports, market. http://www.primaryinfo.com/aluminum_powder.htm accessed December 12, 2018.
Rai, A., Park, K., Zhou, L., Zachariah, M.R., 2006. Understanding the mechanism of aluminium nanoparticle oxidation. Combust. Theor. Model. 10, 843–859.
Retsch, CryoMill. n.d. https://www.retsch.com/products/milling/ball-mills/mixer-mill-cryomill/function-features/. accessed December 12, 2018.
Rufino, B., Boulc'h, F., Coulet, M.-V., Lacroix, G., Denoyel, R., 2007. Influence of particles size on thermal properties of aluminium powder. Acta Mater. 55, 2815–2827. https://doi.org/10.1016/j.actamat.2006.12.017.
Rufino, B., Coulet, M.-V., Bouchet, R., Isnard, O., Denoyel, R., 2010. Structural changes and thermal properties of aluminium micro- and nano-powders. Acta Mater. 58, 4224–4232. https://doi.org/10.1016/j.actamat.2010.04.014.
Samperi, F., Puglisi, C., Alicata, R., Montaudo, G., 2004. Thermal degradation of poly(ethylene terephthalate) at the processing temperature. Polym. Degrad. Stabil. 83, 3–10. https://doi.org/10.1016/S0141-3910(03)00166-6.
Sánchez-López, J.C., Caballero, A., Fernández, A., 1998. Characterisation of passivated aluminium nanopowders: an XPS and TEM/EELS study. J. Eur. Ceram. Soc. 18, 1195–1200. https://doi.org/10.1016/S0955-2219(98)00042-9.
Sarathi, R., Sindhu, T.K., Chakravarthy, S.R., 2007. Generation of nano aluminium powder through wire explosion process and its characterization. Mater. Char. 58, 148–155. https://doi.org/10.1016/j.matchar.2006.04.014.
Schaffer, G.B., Hall, B.J., 2002. The influence of the atmosphere on the sintering of aluminum. Metall. Mater. Trans. 33, 3279–3284.
Schaffer, G.B., Hall, B.J., Bonner, S.J., Huo, S.H., Sercombe, T.B., 2006. The effect of the atmosphere and the role of pore filling on the sintering of aluminium. Acta Mater. 54, 131–138.
Siddiqui, M.Z., Park, Y.K., Kang, Y., Watanabe, A., Kim, S., Kim, Y.M., 2019. Effective use of aluminum-plastic laminate as a feedstock for catalytic pyrolysis over micro and mesoporous catalysts. J. Clean. Prod. 229, 1093–1101. https://doi.org/10.1016/j.jclepro.2019.04.404.
Sun, X.K., Cong, H.T., Sun, M., Yang, M.C., 1999. The effect of heat treatment on tensile properties of the cold-compacted nanocrystalline Al. Nanostruct. Mater. 11, 917–923. https://doi.org/10.1016/S0965-9773(99)00391-8.
Suryanarayana, C., 2001. Mechanical alloying and milling. Prog. Mater. Sci. 46, 1–184.
Tepper, F., 2000. Nanosize powders produced by electro-explosion of wire and their potential applications. Powder Metall. 43, 320–322. https://www.scopus.com/inward/record.uri?eid=2-s2.0-0034478418&partnerID=40&md5=e6bbb78edf905d5d37aa28418390bab6.
Tillborg, H., Nilsson, A., Hernnäs, B., Mårtensson, N., Palmer, R.E., 1993. X-ray and UV photoemission studies of mono-, bi-and multilayers of physisorbed molecules: O2 and N2 on graphite. Surf. Sci. 295, 1–12.
Tougaard, S., 2010. Energy loss in XPS: fundamental processes and applications for quantification, non-destructive depth profiling and 3D imaging. J. Electron. Spectrosc. Relat. Phenom. 178–179, 128–153. https://doi.org/10.1016/j.elspec.2009.08.005.
Trudeau, M.L., Schulz, R., Zaluski, L., Hosatte, S., Ryan, D.H., Doner, C.B., Tessier, P., Ström-Olsen, J.O., Van Neste, A., 1992. Nanocrystalline iron-titanium alloys prepared by high-energy mechanical deformation. In: Mater. Sci. Forum. Trans Tech Publ, pp. 537–544.
Urbonavicius, M., Varnagiris, S., Girdzevicius, D., Milcius, D., 2017. Hydrogen generation based on aluminum-water reaction for fuel cell applications. Energy Procedia 128, 114–120.
Vorozhtsov, A.B., Lerner, M., Rodkevich, N., Nie, H., Abraham, A., Schoenitz, M., Dreizin, E.L., 2016. Oxidation of nano-sized aluminum powders. Thermochim. Acta 636, 48–56. https://doi.org/10.1016/j.tca.2016.05.003.
Williams, J.E., 1984. Production of aluminum powder. Met. Handb. 7, 125–130.
Xie, M., Bai, W., Bai, L., Sun, X., Lu, Q., Yan, D., Qiao, Q., 2016. Life cycle assessment of the recycling of Al-PE (a laminated foil made from polyethylene and aluminum foil) composite packaging waste. J. Clean. Prod. 112, 4430–4434. https://doi.org/10.1016/j.jclepro.2015.08.067.
Ye, J., Schoenung, J.M., 2004. Technical cost modeling for the mechanical milling at cryogenic temperature (cryomilling). Adv. Eng. Mater. 6, 656–664. https://doi.org/10.1002/adem.200400074.
Yin, S., Rajarao, R., Gong, B., Wang, Y., Kong, C., Sahajwalla, V., 2019. Thermo-delamination of metallised composite plastic: an innovative approach to generate Aluminium from packaging plastic waste. J. Clean. Prod. 211, 321–329. https://doi.org/10.1016/j.jclepro.2018.11.158.
Yin, S., Rajarao, R., Gong, B., Wang, Y., Kong, C., Sahajwalla, V., 2019. Thermo-delamination of metallised composite plastic: an innovative approach to generate Aluminium from packaging plastic waste. J. Clean. Prod. 211, 321–329.